Live imaging of root–bacteria interactions in a microfluidics setup

Hassan Massalha[a], Elisa Korenblum[a], Sergey Malitsky[a], Orr H. Shapiro[a,b,1], and Asaph Aharoni[a,1]

[a]Department of Plant and Environmental Sciences, Weizmann Institute of Science, Rehovot 76100, Israel; and [b]Department of Food Quality and Safety, Institute for Postharvest and Food Sciences, Agricultural Research Organization, The Volcani Center, Rishon LeZion 7528809, Israel

Edited by Natasha V. Raikhel, Center for Plant Cell Biology, Riverside, CA, and approved March 2, 2017 (received for review December 8, 2016)

Plant roots play a dominant role in shaping the rhizosphere, the environment in which interaction with diverse microorganisms occurs. Tracking the dynamics of root–microbe interactions at high spatial resolution is currently limited because of methodological intricacy. Here, we describe a microfluidics-based approach enabling direct imaging of root–bacteria interactions in real time. The microfluidic device, which we termed tracking root interactions system (TRIS), consists of nine independent chambers that can be monitored in parallel. The principal assay reported here monitors behavior of fluorescently labeled *Bacillus subtilis* as it colonizes the root of *Arabidopsis thaliana* within the TRIS device. Our results show a distinct chemotactic behavior of *B. subtilis* toward a particular root segment, which we identify as the root elongation zone, followed by rapid colonization of that same segment over the first 6 h of root–bacteria interaction. Using dual inoculation experiments, we further show active exclusion of *Escherichia coli* cells from the root surface after *B. subtilis* colonization, suggesting a possible protection mechanism against root pathogens. Furthermore, we assembled a double-channel TRIS device that allows simultaneous tracking of two root systems in one chamber and performed real-time monitoring of bacterial preference between WT and mutant root genotypes. Thus, the TRIS microfluidics device provides unique insights into the microscale microbial ecology of the complex root microenvironment and is, therefore, likely to enhance the current rate of discoveries in this momentous field of research.

TRIS | live-imaging microscopy | root–bacteria interaction | *Bacillus subtilis* | microbial community dynamics

Plant roots are among the most productive ecosystems in the topsoil layer. The unique conditions formed within the rhizosphere (i.e., the few millimeters of soil extending from the root surface) foster numerous interkingdom interactions shaped through long evolutionary history (1–3). Plant roots receive a multitude of signals and depending on their physiological state, respond by secretion of various exudates through their outer layer (4, 5). These exudates lead to chemical and physical modifications of the rhizosphere microenvironment. The unique conditions found within the rhizosphere exert a strong selection pressure on the diverse microbial communities associated with the surrounding soils, resulting in the enrichment of specific microbial populations that have evolved to colonize the root surface (2, 6, 7). Although many past studies described pathogenic interactions (8), recent work revealed multiple beneficial effects of root-associated bacteria. In agricultural crops, such beneficial bacteria have the potential to positively impact crop yields by improving plant fitness or through the elimination of root pathogens (9–12). Thus, improved understanding of root–bacteria interactions is of major interest to both basic and applied plant research.

Conditions within the rhizosphere are highly heterogeneous in both space and time. Metabolic profiling of *Arabidopsis thaliana* root exudates revealed a diverse chemical repertoire, including organic acids, amino acids, dipeptides, and secondary metabolites (13). Single-cell type analysis of *Arabidopsis* root metabolites showed that different tissues exhibit unique metabolic profiles (14). Thus, root exudate composition likely varies along the length of the root and over the course of root development (15–17). Correspondingly, studies of root bacterial colonization detected specific bacterial species associated with different parts of the embryonic root tissue (15). Nevertheless, current approaches for studying root–bacteria interactions are limited in their capacity to track changes in bacterial colonization of the root surface over space and time and even more to examine bacterial behavior underlying these colonization patterns.

Microfluidic approaches in combination with advanced microscopy provide a powerful set of tools for studying biological systems at the microscale (18). System miniaturization enables precise control over environmental parameters within the system, while allowing direct observation of dynamic biological processes at high spatial–temporal resolutions. Several microfluidic approaches have recently been adapted for use in the plant sciences (reviewed in ref. 19), particularly for the study of root development and physiology (20–22), offering a promising alternative to conventional methods used in the field. Only a single study investigated plant root–microorganism interaction with microfluidics, observing nematode root penetration and hyphae attraction to roots (23). However, root–bacteria interaction dynamics was not observed in such a setup to date. Application of microfluidics-based technologies for investigating bacterial behavior and colonization dynamics at the root interface will provide an indispensable tool in the rapidly evolving field of rhizosphere microbiology (24, 25).

Here, we developed a relatively simple and efficient microfluidic-based system for tracking root–bacteria interaction in real time. The microfluidic device, which we termed tracking root interactions

Significance

Microbial interactions in the rhizosphere, the microenvironment surrounding plant roots, are a major research area for both plant biologists and microbial ecologists. A significant obstacle in this field is the difficulty in studying root–bacteria interactions in real time. Here, we developed a microfluidics-based device that allows dynamic imaging of root–bacterial interactions at previously unattainable spatiotemporal resolutions. The intimate interaction of *Bacillus subtilis* with plant roots is accurately traced in high resolution to the root elongation zone. We further reveal how bacterial behavior leads to rapid root colonization and exclusion of competing bacteria. Hence, this approach has the potential to transform our understanding of root–bacteria interactions and the modulation of bacterial communities colonizing the root surface.

Author contributions: H.M., O.H.S., and A.A. designed research; H.M., E.K., and S.M. performed research; H.M., O.H.S., and A.A. analyzed data; and H.M., O.H.S., and A.A. wrote the paper.

The authors declare no conflict of interest.

This article is a PNAS Direct Submission.

[1]To whom correspondence may be addressed. Email: orr@agri.gov.il or asaph.aharoni@weizmann.ac.il.

This article contains supporting information online at www.pnas.org/lookup/suppl/doi:10.1073/pnas.1618584114/-/DCSupplemental.

system (TRIS), allows up to nine independent assays of *Arabidopsis* seedlings. Roots of individual seedlings grow into individual microfluidic chambers, in which they are inoculated with selected bacterial strains and imaged using wide-field or confocal microscopy. This platform allows direct observation and study of bacterial behavior with a living plant root under specific physical and chemical environmental conditions. It, therefore, provides unique insights into the microscale microbial ecology of this complex environment.

The applicability of our method was shown by real-time imaging of the interaction between the soil-borne bacterium *Bacillus subtilis* and actively growing *Arabidopsis* roots. *B. subtilis* is an established model for root-associated bacteria, well-known for its ability to colonize plant roots and induce beneficial effects on plant growth (26–28). Using the TRIS microfluidic device, we observed a unique pattern of *B. subtilis* attraction directed toward a specific region of the growing root. We further discovered that *B. subtilis* actively excludes *Escherichia coli* from the root surface, indicating a possible protection mechanism against root pathogens. Finally, we assembled and applied a modified version of the TRIS device, allowing the simultaneous tracking of two root systems in a single chamber built to study bacterial preference between WT and mutant root genotypes. These experiments showed that the combination of microfluidics and live-imaging microscopy is a powerful method for studying root–bacteria interactions.

Results

Microfluidic Device Assembly and Experimental Setup. To visualize root–bacteria interaction in real time, we explored the possibility of developing a microfluidic-based system that allows tracking bacteria in high resolution at the root interface. We fabricated TRIS, a microfluidic device that, after it is coupled to the appropriate microscopy and image analysis techniques, provides high spatial and temporal resolution information vis-à-vis bacterial behavior in a root environment. The TRIS device allows monitoring of individual *Arabidopsis* roots in nine separate channels (Fig. 1). To prevent cross-contamination between channels throughout bacterial inoculation, each channel contains independent inlet and outlet ports. A third port, located at one end of the channel, is used for introduction of the germinated *Arabidopsis* root. Channels are etched by soft lithography into a single slab of polydimethylsiloxane (PDMS) bonded to a glass microscope slide (29, 30). The design consists of an elongated hexagon with a short extension at one end, with outer dimensions of 13 × 4 mm (Fig. S1). The total internal volume of the channels is ∼6.4 μL, and their height is set to 160 μm, providing ample space for growth of roots having a typical diameter of 100 μm. Roots of up to 8 mm in length could be grown in each channel (i.e., up to 10 d from germination in the case of *A. thaliana*). *Arabidopsis* seeds are first germinated in agar-filled pipette tips, which are subsequently placed at the dedicated port of each channel, and the device is incubated for up to 5 d under appropriate conditions (*Materials and Methods*). After root elongation, the device is placed on a microscope stage, with polyethylene tubes connected to the inlet and outlet ports for liquid handling and inoculation with bacteria (Fig. 1 and Fig. S2). A custom humidity chamber is used to minimize liquid evaporation during long-term imaging. This setup allows for capturing the dynamic behavior of bacteria at and around the root surface under controlled conditions with high spatial and temporal resolutions.

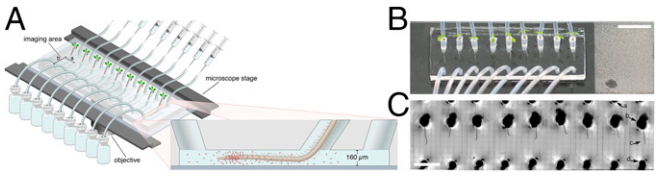

Fig. 1. TRIS: a microfluidic device for tracking root–bacteria interactions. (*A*) Illustration of the TRIS device mounted on the microscope stage (dark rim). (*Inset*) Schematic longitudinal section of a microfluidic channel containing root and bacterial cells (red; not drawn to scale). (*B*) Top view of *Arabidopsis* seedlings growing in plastic pipette tips attached to the TRIS device. Roots are visible as thin white lines extending from tip ends. (Scale bar: 1 cm.) (*C*) Microscopic view of nine *Arabidopsis* roots growing inside the TRIS microfluidic device captured using bright-field illumination at 10× magnification. Arrows: *a*, inlet port.; *b*, tip in a root-dedicated port with *c*, root extending toward the outlet port; *d*, outlet port. (Scale bar: 5 mm.)

TRIS Enables Real-Time Imaging of Bacterial Attraction and Root Surface Colonization. *B. subtilis* is known to effectively colonize the surface of growing roots, including that of *Arabidopsis* (31). To study the initiation of this process, we injected 10^6 cells per 1 mL fluorescently labeled *B. subtilis* into the TRIS microfluidic system using preloaded syringes. Bacterial behavior was studied over the next 30 min using video microscopy with dark-field illumination. We consistently observed rapid bacterial accumulation at an area just above the root tip, likely driven by chemotaxis toward high local concentrations of root exudates (Fig. 2*A*). This behavior is evident already 20 min postinoculation, a period considerably shorter than the bacterial doubling time of ∼24 min in a rich media (Fig. S3), indicating that bacterial accumulation at this stage is not driven by bacterial growth. This bacterial "hotspot" remained noticeable over at least 30 min, with bacterial cells continuing to accumulate throughout the imaging period.

To extend the observation of root colonization over periods of several hours, we combined the TRIS microfluidic setup with laser-scanning confocal microscopy. Using time-lapse microscopy, we followed bacteria–root interactions of nine independent inoculations at 30-min intervals over a period of 12 h. Bacterial accumulation immediately above the root tip was observed already 30 min from inoculation exactly. Bacterial density at the same position increased significantly by fivefold during the first 6 h postinoculation (Fig. 2*B* and Movie S1). Interestingly, after 6 h, we observed a gradual decrease of bacterial density above the root tip and concomitant bacterial accumulation appearing as large bacterial plugs (likely showing biofilm formation) on the root surface farther from the growing tip (Fig. 2*B*). Interestingly, the time window of the observed reduction is in line with a recent study, suggesting that the primary adhesion of bacterial cell to root surface would likely be reversible before cellular specification in production of ECM (32).

On surface interaction, bacteria are known to secrete ECM largely composed of exopolysaccharides (EPSs), proteins, and nucleic acids that lead to formation of a biofilm layer (33). To examine more precisely the time and location of biofilm formation on the root surface in the course of root–bacteria interactions, we used an EPS bacterial mutant (*eps*) that has a defect in its ability to form biofilm. Cells of the *eps* mutant showed strong and specific attraction above the growing tip, similar to that displayed by the WT strain. However, bacterial colonization over the entire root length, observed during the later stages of the original experiment (from 3 to 4 h and on), was significantly reduced (Fig. 2*C* and Movie S2).

Another aspect of using the TRIS-based method for root interaction studies is the possibility to simultaneously visualize different fluorescent reporters derived from roots as well as the interacting organism: here, bacterial cells. We used a set of GFP-labeled *Arabidopsis* lines, each marking a different root cell type, to determine precisely the root zone targeted by *B. subtilis* attraction. Using the same setup portrayed above, we tracked bacterial attraction to the roots of six *Arabidopsis* cell type marker lines expressing a GFP reporter, including COBRA-LIKE9 (COBL9; delineating the root hairs), CORTEX (cortex), WER (nonhair epidermis), SCARECROW (SCR; endodermis-quiescent center), WOODEN LEG (WOL; vasculature), and PET111 (columella) (Fig. 3). Results from these experiments specified that *B. subtilis* cells are primarily attracted toward the

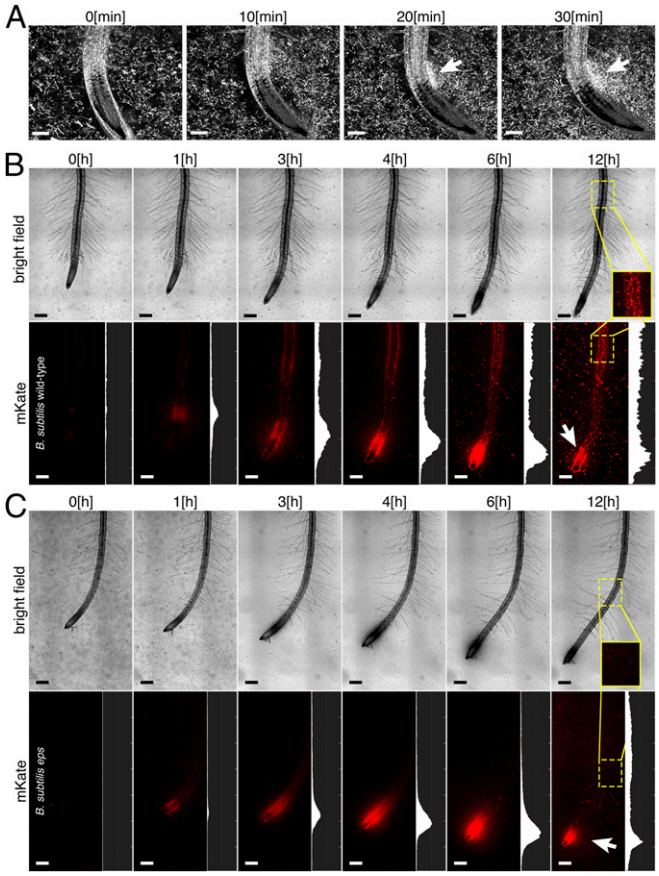

Fig. 2. Live imaging of *B. subtilis* cells interaction with *Arabidopsis* root. (*A*) Accumulation of *B. subtilis* cells near the root elongation zone of *Arabidopsis* seedlings (white arrows) during the first 30 min of coincubation. Each image is an MIP from a short video (11 s; ~100 frames) obtained using dark-field microscopy. The rapid accumulation suggests a chemotactic response of bacterial cells toward high local concentrations of root exudates. (*B*) Selected images from time-lapse confocal microscopy of a WT *Arabidopsis* root (bright field) incubated with red fluorescent-labeled *B. subtilis* (mKate) for 12 h. Images are representative of nine independent inoculation experiments. (*C*) A *B. subtilis* biofilm defective mutant (*eps*) shows similar attraction as the WT strain but with little or no subsequent biofilm formation. Images are representative of four independent inoculation experiments. The white area plots (on the right side of the mKate fluorescent images) show normalized bacterial quantification. These area plots could be compared between the experiments in *B* and *C*; *x* axes in all area plots have the same length and range between zero and one normalized intensity. (*Insets* in *B* and *C*) Higher magnification view of the area marked by a dashed box in the mKate view. The same area is marked by a dashed box in the bright-field view. Magnification in *B* shows biofilm formation at a mature part of the root compare to *C*. White arrows in *B* and *C* indicate lower bacterial accumulation, likely because of a lower amount of motile cells at 12 h (compared with the same area at 6 h). (Scale bars: 200 μm.)

border region between the root elongation and early maturation zones. The upper limit of this zone was delineated by the GFP fluorescence of the COBL9 line as well as the higher GFP intensity of the CORTEX marker. This observation was further supported by tracking the upper part of the WER signal, displaying preferential expression pattern in the lateral root cap cells adjacent to the elongation zone (34) (Movies S3–S5). The lower border of the *B. subtilis* cells attraction zone was defined by the root meristematic cell niche marker SCR as well as the columella marker (PET11), both located below the root elongation zone. Interestingly, this section of the root marked by the two reporters, SCR and PET111, is initially not colonized by *B. subtilis* cells over the first 2 h of the experiment. The latter observation was supported by the *WOL* and *WER* (its lower part) markers. *SCR* cells are located in the midplane of the root, one cell layer below the *WOL* cells, and medial to the cells marked by *WER*, marking the meristematic zone in the *Arabidopsis* root. By integrating the information from these cell type markers, we could confidently define the hotspot for *B. subtilis* attraction as the root elongation zone. Moreover, the maximum ratio of bacterial density of the root "young part" vs. the "mature part" (approximately twofold) was observed at 6 h postinoculation (Fig. S4) as detected in the independent experiment described above (Fig. 2). In addition to the significant accumulation of bacteria at the elongation zone, we also detected low but significant accumulation at lower root regions during later stages of these experiments (after 4–5 h postinoculation) (Fig. 3 and Movies S6–S8), indicating an additional root–bacteria interaction process.

Bacterial Competition for Domination of the Root Surface. The nutrient-rich microenvironment created by plant roots drives a fierce competition between cohabiting soil microorganisms (35–37). This type of interaction is of particular importance when considering the infiltration of the rhizosphere microbiome by root pathogens. We used the TRIS system to examine in real-time bacteria–bacteria interaction in the presence of roots. Thus, *Arabidopsis* roots were inoculated with fluorescently tagged cells of *E. coli* with or without the addition *B. subtilis*. *E. coli* is a Gram-negative bacterium and can be found in temperate soil or as a result of manure fertilization (38, 39). Moreover, *E. coli* strains isolated from plant roots are found to harbor traits indicative for root association, such as biofilm formation and

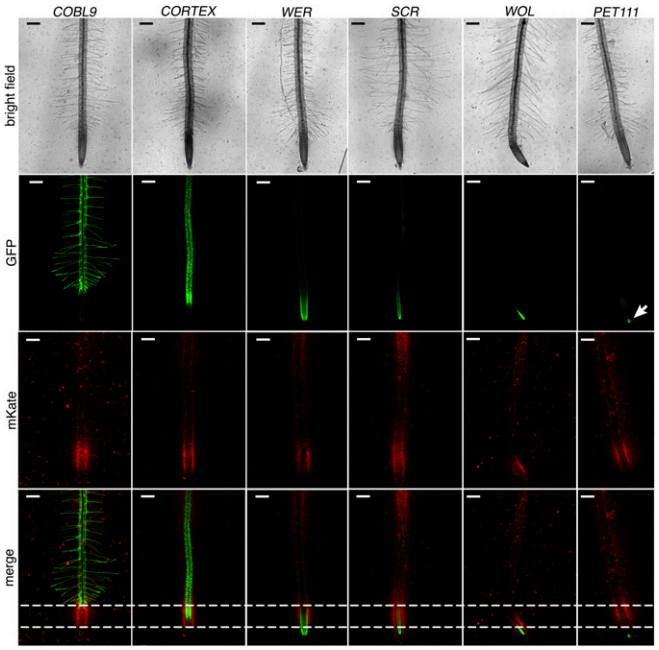

Fig. 3. *B. subtilis* is attracted to the root elongation zone. Single images extracted from a time-lapse image series of six *Arabidopsis* strains with a constitutive GFP reporter (green) marking different root cell types. Each strain was incubated with fluorescently labeled (mKate) *B. subtilis* cells (red). GFP labeling is in the following root cell types: root hairs (COBL9), cortex (CORTEX), nonhair epidermis (WER), endodermis-quiescent center (SCR), vasculature (WOL), and columella (PET111). The presented images were obtained 2 h after introducing labeled *B. subtilis* into the TRIS device. The two horizontal dashed lines in the merge row denote the region of primary bacterial colonization. The white arrow in the PET111 GFP image points to the green fluorescent signal coming from the columella cell type. One set of images was presented of three independent experiments for each reporter line. (Scale bars: 200 μm.)

utilization of aromatic compounds likely found in plant tissues (40). When inoculated alone, *E. coli* seemed to have a markedly different root colonization pattern compared with the one of *B. subtilis*. Cells of *E. coli* are typically dispersed homogeneously along the entire root length, with minor accumulation at the root cap starting at 3 h postinoculation (Fig. 4*A* and Movie S9). However, this pattern changed dramatically after *E. coli* and *B. subtilis* were coinoculated. Although *B. subtilis* followed a similar colonization pattern to the one described above, cells of *E. coli* were effectively excluded from the root surface within 3 h of inoculation. The bulge-shaped *E. coli* "exclusion" area started at the root elongation zone, where *B. subtilis* predominantly colonizes to the highest densities. By the end of the experiment (12 h postinoculation), the exclusion zone was further extended to over 100 μm from the root surface (Fig. 4*B* and Movie S10). Relative quantification of bacterial fluorescence intensity showed a strong negative correlation between *B. subtilis* and *E. coli* concentrations (Fig. 4*C*, *SI Materials and Methods*, and Fig. S5).

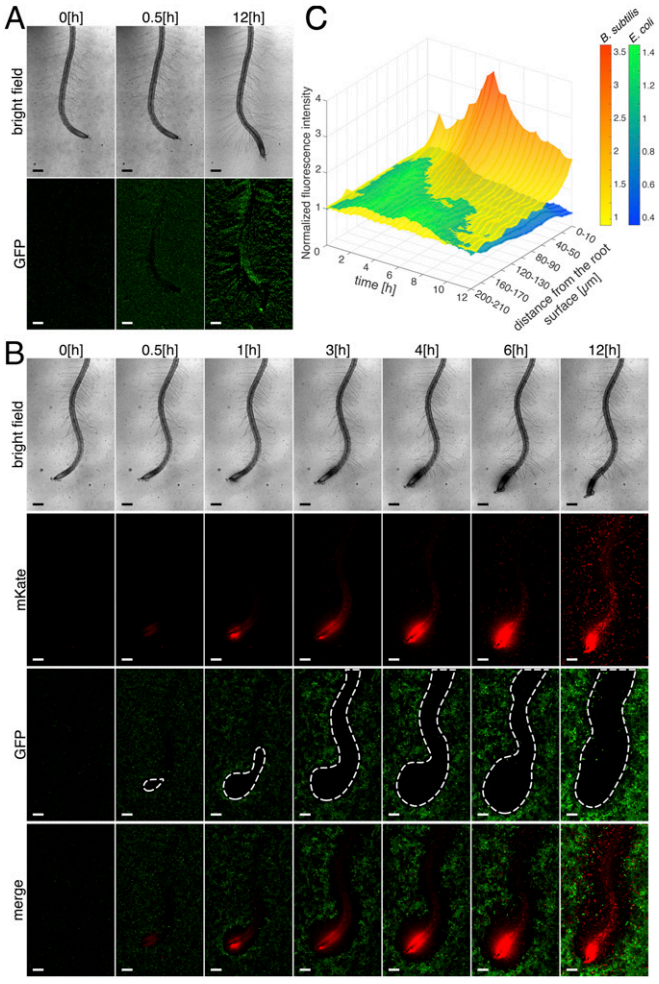

Fig. 4. Bacterial competition for root surface colonization. Real-time imaging of two bacterial strains at the root zone. (*A*) WT *Arabidopsis* root (bright field) inoculated with *E. coli* cells (GFP) and imaged every 30 min for 12 h. Images are representative of five independent inoculation experiments; Movie S9 shows the complete experiment. (*B*) WT *Arabidopsis* root (bright field) coincubated with a mixture of GFP-labeled *E. coli* (green) and mKate-labeled *B. subtilis* (red). White dashed lines in the GFP images delineate the exclusion zone of the *E. coli* from the root. Images are representative of four independent coinoculation experiments. (*C*) Quantification of normalized bacterial fluorescence intensity in *B* at each time point of *B. subtilis* (red–yellow surface) and *E. coli* (green–blue surface) as a function of the distance from the root surface over 12 h. (Scale bars: 200 μm.)

Importantly, cell densities of *B. subtilis* within the exclusion zone were similar to those measured beyond it, suggesting that the exclusion of *E. coli* is likely mediated by diffusible agents exuded by either colonized root or *B. subtilis* in a biofilm structure.

Bacterial Choice Assays in a Double-Channel TRIS Device. A modified double-channel version of our original TRIS microfluidic device was manufactured, consisting of a wider chamber partitioned by a semipermeable divider. This microfluidic device enables the simultaneous observation of two *Arabidopsis* roots growing on each side of the divider in a single background. The divider (exhibiting a pore size of 50 μm) prevents entanglement of the two roots to avoid physical communication between the two plants, while allowing the free flow of bacterial cells and diffusible signaling molecules between the two root systems (Fig. S1*B*).

To show the effectiveness of the double-channel microfluidic device, we tested the preference of *B. subtilis* to either WT *Arabidopsis* or two known root architecture mutants: the hairless *caprice*/*triptychon* (*cpc*/*try*) and the excessive root hair *werewolf*/*myb23* (*wer*/*myb23*) genotypes (41, 42). When comparing two WT plants, *B. subtilis* accumulation around the two root systems was similar in time, with only a minor difference in intensity (Fig. S6 *A* and *D* and Movie S11). In contrast, maximum bacterial accumulation around the two root architecture mutants was reproducibly detected approximately 1 h earlier than for the WT genotype (Fig. S6 *B*, *C*, *E*, and *F* and Movies S12 and S13). Interestingly, significant bacterial accumulation on the hairless mutant root (*cpc*/*try*) was 30% higher than on the WT root when grown side by side in the double-channel device. These results showed the utility of the double-channel device in performing real-time bacterial choice assays and tracking bacterial behavior when exposed to adjacent root systems growing at identical surroundings.

Discussion

The TRIS microfluidic device reported here offers a robust platform for microscopy-based studies of the interactions between roots and associated microorganisms. Real-time microscopic study of roots is typically limited by the opaque soil surrounding the root, and hence, microfluidics offers an attractive solution to such limitation. Although several platforms for live imaging of plant roots have been reported, they were restricted to observations of root systems (43), but none of them showed their immense value in tracking the dynamics of root interactions with other organisms, particularly bacteria. The TRIS device exhibits two key variations compared with the previously reported RootChip platform (22). The RootChip design uses a two-layer design with a built-in valve system to divide a single fluid input into the different channels. Although this design has several advantages in terms of liquid handling, it does not allow liquid separation between the different channels. We thus opted for a different design, with each channel receiving an independent input, enabling the inoculation of roots with different microbial communities with no cross-contamination. This design also allowed us to implement the device in a single PDMS layer, which in turn, permits easier fabrication, experiment assembly, and operation. Thus, TRIS offers a robust microfluidic platform for studying root–bacteria interactions that can be implemented in a typical experimental biology laboratory.

Experiments involving different organisms (i.e., a plant root and bacteria) spanning three orders of magnitude in scale makes image acquisition a challenging task. Furthermore, bacterial cells are motile, able to move on surfaces because of swarming, and act as a community. Therefore, an optimized scanning procedure is required to follow maximal bacterial behavioral dynamics on the one hand, while scanning multiple roots in parallel (up to nine in our typical setup) on the other hand. Whereas shorter time intervals between frames will permit the analysis of fewer roots per experiment, longer time intervals will result in less accurate measurement of bacterial behavior surrounding the root. Nevertheless, speeding up image acquisition can be likely

achieved by the use of light-sheet microscopy through a lower sample laser exposure rate (44).

The application of the TRIS platform was shown for studying three fundamental questions in root–bacteria interactions. Using our principal microfluidic design, we investigated the initiation of bacterial colonization of the root surface as well as competition between different bacterial species. We used a second fluidics design, incorporating two root systems in a single chamber, to examine the ability of bacteria to distinguish between roots of different plant genotypes. These preliminary experiments provided unique insights into the microscale features of the root interaction domain. Perhaps the most robust of these observations was the initial aggregation of *B. subtilis* at the elongation zone of *Arabidopsis* roots. This accumulation is strikingly observed already 20 min postbacterial inoculation, much faster than the expected generation time of *B. subtilis* under the incubation conditions used in these experiments. We thus put forward the hypothesis that this process is primarily driven by bacterial chemotaxis toward exudates secreted from the root surface. The fact that aggregation is only seen at the root elongation zone suggests increased secretion of specific infochemicals from this part of the root, which mediate this attraction (45). Preliminary metabolomics analysis of root exudates performed in the course of this study by analyzing the content of the TRIS device identified several amino acids known to serve as chemoattractants for *B. subtilis* cells (Fig. S7) (46, 47). This result is consistent with a significant reduction in attraction to *Arabidopsis* root shown by *B. subtilis* mutants lacking the chemoreceptors McpB and McpC, known to bind primary metabolites, including amino acids, sugars, and sugar alcohols (32). A thought-provoking link exists between our observations here and a recent report showing Ca^{2+} flux at the root elongation zone on exposure to bacterial proteins (48), signifying that bacteria–root interactions at this localization may involve a two-way communication.

Coinoculation experiments showed active exclusion of *E. coli* from the root surface after its colonization by *B. subtilis*. Interestingly, although *B. subtilis* cells were most concentrated on the root itself, *E. coli* cells were excluded to a distance exceeding 100 μm from the root surface. This pattern indicates that a diffusible agent released from the colonized root or the colonizing bacteria likely mediates the antagonistic interaction. An induction of either production or release of this agent on root colonization may account for the observed expansion of the exclusion zone over the first 4 h of the experiment. One possible mechanism of *E. coli* exclusion could be through diffused molecules released from colonizing *B. subtilis* cells or alternatively, ones secreted from the root on *B. subtilis* colonization. *B. subtilis* biofilms are known to secrete the lipopeptide surfactin, which has antimicrobial effect that might generate the observed *E. coli* exclusion zone (49–51). A recent study showed that an extracellular death factor, a hexapeptide (RGQQNE), secreted by *B. subtilis* cells during chemotaxis was sufficient to activate the toxin–antitoxin system and induce programed cell death in *E. coli* cells (52). Additional investigation using the TRIS platform, including chemical and proteomic analyses of root exudates as well as assays with surfactin defective mutants, will likely clarify the nature of the observed bacterial species interaction in the presence of roots.

Using the double-channel design, we could measure bacterial preference for specific root genotypes. Bacterial preference can be regarded as a measurement of the ability of a plant to recruit microbes from the environment. Here, we show the effect of the two main regulatory transcription factors, *wer myb23* and *cpc try*, that control root hair formation on bacterial accumulation. *B. subtilis* showed an increased affinity toward the architectural mutant roots represented in the early colonization and higher bacterial intensity developed by time, in particular, *cpc try*, compared with the WT. The elongation zone is well-described as the location at which cells will either develop as a root hairs or remain as epidermis cell (53, 54). Thus, changes in root hair differentiation might be responsible for the altered bacterial attraction that we observed in the double TRIS assay. More profound research is required to identify the mechanisms underlying the observed differences between bacterial attraction and accumulation on surfaces of mutant plants altered in root architecture.

The use of the TRIS device here represents only a small portion of the expected applications of this method in studying root interactions. This system may be extended for studying, for example, plant–plant and not merely plant–bacteria interactions. Endless combinations of bacterial strains and plant genotypes could be examined with multiple fluorescent reporters. Altogether, we anticipate that the reported method will open the way for extensive high-resolution spatial–temporal studies of bacterial dynamics in the root environment.

Materials and Methods

Plant Material and Growth. WT *A. thaliana* ecotype Columbia (Col-0) seedlings were grown as described by Grossmann et al. (22) with minor modifications. In short, seeds were surface sterilized in chlorine gas for 2 h in a closed desiccator and transferred aseptically to a plastic pipette tip (one seed per tip) containing one half-strength Murashige and Skoog basal salt mixture (Duchefa Biochemie) supplemented with 0.8% (wt/vol) plant agar (Duchefa Biochemie) and without sugar supplement. The seed-containing tips were preincubated at 4 °C for 48 h in the dark and transferred to a 16-h light/8-h dark period at 23 °C for 3–4 d. Plastic tips with growing seedlings were placed in the TRIS device and incubated vertically for an additional 4–5 d before imaging. All mutant lines and cell layer markers were in the Col-0 background.

Microbial Strains and Culture Conditions. *B. subtilis* strain NCIB 3610 and the EPS mutant (*eps*; strain 3610 background) were mKate labeled, and *E. coli* OKN3 GFP-labeled was inoculated in 1% (wt/vol) tryptone and 0.5% (wt/vol) NaCl, pH 7 (Sigma; TB buffer) overnight at 37 °C, diluted 1:100 into fresh TB buffer the next day, and incubated again in the same conditions to reach OD_{600} of 0.6. The cells were washed twice gently with plant media (Murashige and Skoog), suspended in Murashige and Skoog, and kept 30 min at room temperature before applying to *Arabidopsis* roots in the TRIS device. *B. subtilis* growth under relevant conditions was assessed by incubation in either Lysogeny broth or Murashige and Skoog. Bacterial density was measured at OD_{600} every 15 min for 13 h in a plate reader (BioTek; $n = 5$ for each individual point).

TRIS Design and Assembly. TRIS microchannels were fabricated in PDMS (Dow Croning) using lithography and replica molding. *SI Materials and Methods* has technical details.

Setup of the TRIS Assay. Autoclaved mounted microfluidic devices were filled with liquid plant media (one half-strength basal salt Murashige and Skoog without agar and sugar supplements) carefully to eliminate air bubbles trapped in the system in sterile conditions. Plastic tips containing growing seedlings were placed in the root hole of each channel of the microfluidic device and incubated for 4–5 d in the growth room. On the day of imaging, each microchannel was connected with two polypropylene tubes (1.2 mm o.d.) to the inlet and outlet holes. The tubes were filled with Murashige and Skoog media before connecting them to the TRIS device using 18-gauge needles. Plastic syringes (1-mm volume) filled with washed bacterial cell suspension were connected to the inlet tube to inoculate the chambers. Reservoir tubes (Eppendorf) filled with Murashige and Skoog were connected to the other end of the second tube. Finally, the fully connected TRIS device was mounted onto a microscope stage and covered with a plastic cover containing a transparent window to maintain a humid environment for the *Arabidopsis* seedlings. The room was temperature controlled and set to 23 °C (Fig. 1 and Fig. S2). After setting the channel position coordinates in the microscope software, the *z* axis was adjusted to the midplane of each root. Mounting the microfluidic device to a standard microscope slide makes it suitable for different imaging platforms. Images were taken with either dark-field or confocal microscopy. After the microfluidic device was fixed to the microscope stage and imaging parameters were adjusted, bacterial cells were introduced to the TRIS device. Quality control and other experimental tips are in *SI Materials and Methods*.

Image Acquisition and Dark-Field Microscopy Analysis. An inverted optical microscope (Olympus) equipped with a 10× dark-field objective was used to record bacterial dynamics. After the TRIS device was properly mounted as

mentioned above, root midplane was selected manually for image acquisition. *B. subtilis* cells were injected into the TRIS device, denoted as $t = 0$. Short videos (~100 frames) were captured at a frame rate of approximately nine frames per second, each 5 min, up to 30 min postinoculation. Image analysis was done in two steps using built-in functions in the cellSens software (Olympus): (*i*) background subtraction from all acquired frames and (*ii*) generation of a maximum intensity projection (MIP) image of the captured videos for each time point.

Confocal Image Acquisition and Analysis. An inverted laser-scanning confocal microscope (Nikon Corporation) Ti-eclipse body equipped with a 10× objective lens (CFI Plan Fluor 10×; N.A. 0.3) and an automated stage was used to track long-term fluorescent bacterial behavior. The microscope was programed to scan multiple roots at three *z* slices (40-μm distance from one to the other) of large images (6.5 × 7.5 mm) each 30 min postbacterial inoculation ($t = 0$) for 12 h in dark light conditions. Laser illumination emission at 488 nm coupled with a 525/50-nm excitation filter was used for GFP fluorescence, and laser illumination of 561 nm coupled with a 595/50-nm excitation filter was used for mKate fluorescence. Images were exported as tiff files and processed in Matlab (Mathworks). Image analysis is in *SI Materials and Methods* and Figs. S8 and S9.

Metabolomics Analysis of the TRIS Device Content. Information is in *SI Materials and Methods*.

ACKNOWLEDGMENTS. We thank I. Kolodkin-gal for fruitful discussions and providing the *B. subtilis* lines; O. Bitton, L. Tunik, and A. Yoffe for assistance in the nanofabrication facility; and P. Benfey for cell layer reporters and the root mutants. We also thank the Adelis Foundation, the Leona M. and Harry B. Helmsley Charitable Trust, the Jeanne and Joseph Nissim Foundation for Life Sciences, the Tom and Sondra Rykoff Family Foundation Research, and the Raymond Burton Plant Genome Research Fund for supporting the activity of the laboratory of A.A. This research was supported as part of a PhD funded by a Planning & Budgeting Committee of the Council of Higher Education of Israel personal grant (to H.M.). A.A. is the incumbent of the Peter J. Cohn Professorial Chair.

1. Tkacz A, Cheema J, Chandra G, Grant A, Poole PS (2015) Stability and succession of the rhizosphere microbiota depends upon plant type and soil composition. *ISME J* 9: 2349–2359.
2. Bulgarelli D, et al. (2012) Revealing structure and assembly cues for Arabidopsis root-inhabiting bacterial microbiota. *Nature* 488:91–95.
3. Tringe SG, et al. (2005) Comparative metagenomics of microbial communities. *Science* 308:554–557.
4. Lundberg DS, et al. (2012) Defining the core Arabidopsis thaliana root microbiome. *Nature* 488:86–90.
5. Haney CH, Samuel BS, Bush J, Ausubel FM (2015) Associations with rhizosphere bacteria can confer an adaptive advantage to plants. *Nat Plants* 1:15051.
6. Ofek-Lalzar M, et al. (2014) Niche and host-associated functional signatures of the root surface microbiome. *Nat Commun* 5:4950.
7. Lebeis SL, et al. (2015) PLANT MICROBIOME. Salicylic acid modulates colonization of the root microbiome by specific bacterial taxa. *Science* 349:860–864.
8. Ryan RP, et al. (2011) Pathogenomics of Xanthomonas: Understanding bacterium-plant interactions. *Nat Rev Microbiol* 9:344–355.
9. Weyens N, van der Lelie D, Taghavi S, Vangronsveld J (2009) Phytoremediation: Plant-endophyte partnerships take the challenge. *Curr Opin Biotechnol* 20:248–254.
10. Mei C, Flinn BS (2010) The use of beneficial microbial endophytes for plant biomass and stress tolerance improvement. *Recent Pat Biotechnol* 4:81–95.
11. Hardoim PR, van Overbeek LS, Elsas JD (2008) Properties of bacterial endophytes and their proposed role in plant growth. *Trends Microbiol* 16:463–471.
12. Santhanam R, et al. (2015) Native root-associated bacteria rescue a plant from a sudden-wilt disease that emerged during continuous cropping. *Proc Natl Acad Sci USA* 112:E5013–E5020.
13. Strehmel N, Böttcher C, Schmidt S, Scheel D (2014) Profiling of secondary metabolites in root exudates of Arabidopsis thaliana. *Phytochemistry* 108:35–46.
14. Moussaieff A, et al. (2013) High-resolution metabolic mapping of cell types in plant roots. *Proc Natl Acad Sci USA* 110:E1232–E1241.
15. Ofek M, Hadar Y, Minz D (2011) Colonization of cucumber seeds by bacteria during germination. *Environ Microbiol* 13:2794–2807.
16. Aulakh MS, Wassmann R, Bueno C, Kreuzwieser J, Rennenberg H (2001) Characterization of root exudates at different growth stages of ten rice (Oryza sativa L.) cultivars. *Plant Biol* 3:139–148.
17. Chaparro JM, Badri DV, Vivanco JM (2014) Rhizosphere microbiome assemblage is affected by plant development. *ISME J* 8:790–803.
18. Shapiro OH, Kramarsky-Winter E, Gavish AR, Stocker R, Vardi A (2016) A coral-on-a-chip microfluidic platform enabling live-imaging microscopy of reef-building corals. *Nat Commun* 7:10860.
19. Sanati Nezhad A (2014) Microfluidic platforms for plant cells studies. *Lab Chip* 14: 3262–3274.
20. Jiang H, Xu Z, Aluru MR, Dong L (2014) Plant chip for high-throughput phenotyping of Arabidopsis. *Lab Chip* 14:1281–1293.
21. Englert DL, Manson MD, Jayaraman A (2010) A microfluidic device for quantifying bacterial chemotaxis in stable concentration gradients. *J Vis Exp* 38:2–7.
22. Grossmann G, et al. (2011) The RootChip: An integrated microfluidic chip for plant science. *Plant Cell* 23:4234–4240.
23. Parashar A, Pandey S (2011) Plant-in-chip: Microfluidic system for studying root growth and pathogenic interactions in Arabidopsis. *Appl Phys Lett* 98:263703.
24. Panke-Buisse K, Poole AC, Goodrich JK, Ley RE, Kao-Kniffin J (2015) Selection on soil microbiomes reveals reproducible impacts on plant function. *ISME J* 9:980–989.
25. Mendes R, et al. (2011) Deciphering the rhizosphere microbiome for disease-suppressive bacteria. *Science* 332:1097–1100.
26. Vullo DL, Coto CE, Siñeriz F (1991) Characteristics of an inulinase produced by Bacillus subtilis 430A, a strain isolated from the rhizosphere of Vernonia herbacea (Vell Rusby). *Appl Environ Microbiol* 57:2392–2394.
27. Pandey A, Palni LM (1997) Bacillus species: The dominant bacteria of the rhizosphere of established tea bushes. *Microbiol Res* 152:359–365.
28. Cazorla FM, et al. (2007) Isolation and characterization of antagonistic Bacillus subtilis strains from the avocado rhizoplane displaying biocontrol activity. *J Appl Microbiol* 103:1950–1959.
29. Rusconi R, Garren M, Stocker R (2014) Microfluidics expanding the frontiers of microbial ecology. *Annu Rev Biophys* 43:65–91.
30. Meier M, Lucchetta EM, Ismagilov RF (2010) Chemical stimulation of the Arabidopsis thaliana root using multi-laminar flow on a microfluidic chip. *Lab Chip* 10:2147–2153.
31. Rudrappa T, Czymmek KJ, Paré PW, Bais HP (2008) Root-secreted malic acid recruits beneficial soil bacteria. *Plant Physiol* 148:1547–1556.
32. Allard-Massicotte R, et al. (2016) Bacillus subtilis early colonization of arabidopsis thaliana roots involves multiple chemotaxis receptors. *MBio* 7:e01664-16.
33. Branda SS, Vik S, Friedman L, Kolter R (2005) Biofilms: The matrix revisited. *Trends Microbiol* 13:20–26.
34. Lee MM, Schiefelbein J (1999) WEREWOLF, a MYB-related protein in Arabidopsis, is a position-dependent regulator of epidermal cell patterning. *Cell* 99:473–483.
35. Berg G, Smalla K (2009) Plant species and soil type cooperatively shape the structure and function of microbial communities in the rhizosphere. *FEMS Microbiol Ecol* 68:1–13.
36. Compant S, Clément C, Sessitsch A (2010) Plant growth-promoting bacteria in the rhizo- and endosphere of plants: Their role, colonization, mechanisms involved and prospects for utilization. *Soil Biol Biochem* 42:669–678.
37. Bulgarelli D, Schlaeppi K, Spaepen S, Ver Loren van Themaat E, Schulze-Lefert P (2013) Structure and functions of the bacterial microbiota of plants. *Annu Rev Plant Biol* 64:807–838.
38. Natvig EE, Ingham SC, Ingham BH, Cooperband LR, Roper TR (2002) Salmonella enterica serovar Typhimurium and Escherichia coli contamination of root and leaf vegetables grown in soils with incorporated bovine manure. *Appl Environ Microbiol* 68:2737–2744.
39. Ishii S, Ksoll WB, Hicks RE, Sadowsky MJ (2006) Presence and growth of naturalized Escherichia coli in temperate soils from Lake Superior watersheds. *Appl Environ Microbiol* 72:612–621.
40. Méric G, Kemsley EK, Falush D, Saggers EJ, Lucchini S (2013) Phylogenetic distribution of traits associated with plant colonization in Escherichia coli. *Environ Microbiol* 15:487–501.
41. Kang YH, et al. (2009) The MYB23 gene provides a positive feedback loop for cell fate specification in the Arabidopsis root epidermis. *Plant Cell* 21:1080–1094.
42. Schellmann S, et al. (2002) TRIPTYCHON and CAPRICE mediate lateral inhibition during trichome and root hair patterning in Arabidopsis. *EMBO J* 21:5036–5046.
43. Stanley CE, Grossmann G, i Solvas XC, deMello AJ (2016) Soil-on-a-Chip: Microfluidic platforms for environmental organismal studies. *Lab Chip* 16:228–241.
44. Maizel A, von Wangenheim D, Federici F, Haseloff J, Stelzer EHK (2011) High-resolution live imaging of plant growth in near physiological bright conditions using light sheet fluorescence microscopy. *Plant J* 68:377–385.
45. Beauregard PB, Chai Y, Vlamakis H, Losick R, Kolter R (2013) Bacillus subtilis biofilm induction by plant polysaccharides. *Proc Natl Acad Sci USA* 110:E1621–E1630.
46. Kirby JR, Kristich CJ, Feinberg SL, Ordal GW (1997) Methanol production during chemotaxis to amino acids in Bacillus subtilis. *Mol Microbiol* 24:869–878.
47. Yang Y, et al. (2015) Relation between chemotaxis and consumption of amino acids in bacteria. *Mol Microbiol* 96:1272–1282.
48. Keinath NF, et al. (2015) Live cell imaging with R-GECO1 sheds light on flg22- and chitin-induced transient [Ca(2+)]cyt patterns in Arabidopsis. *Mol Plant* 8:1188–1200.
49. Fernandes PAV, et al. (2007) Antimicrobial activity of surfactants produced by Bacillus subtilis R14 against multidrug-resistant bacteria. *Braz J Microbiol* 38:704–709.
50. Rivardo F, Turner RJ, Allegrone G, Ceri H, Martinotti MG (2009) Anti-adhesion activity of two biosurfactants produced by Bacillus spp. prevents biofilm formation of human bacterial pathogens. *Appl Microbiol Biotechnol* 83:541–553.
51. Nakata K, Koh MM, Tsuchido T, Matsumura Y (2010) All genomic mutations in the antimicrobial surfactant-resistant mutant, Escherichia coli OW66, are involved in cell resistance to surfactant. *Appl Microbiol Biotechnol* 87:1895–1905.
52. Kumar S, Kolodkin-Gal I, Engelberg-Kulka H (2013) Novel quorum-sensing peptides mediating interspecies bacterial cell death. *MBio* 4:e00314-13.
53. Grierson C, Nielsen E, Ketelaarc T, Schiefelbein J (2014) Root hairs. *Arabidopsis Book* 12:e0172.
54. Takatsuka H, Umeda M (2015) Epigenetic control of cell division and cell differentiation in the root apex. *Front Plant Sci* 6:1178.
55. Ntziachristos V (2010) Going deeper than microscopy: The optical imaging frontier in biology. *Nat Methods* 7:603–614.
56. Malitsky S, et al. (2008) The transcript and metabolite networks affected by the two clades of Arabidopsis glucosinolate biosynthesis regulators. *Plant Physiol* 148:2021–2049.